Donor−Acceptor Tubular Nanoaggregates of Cyclic Oligothiophenes. A Theoretical Study

Manuel Garcia, Estrella Ramos, Patricia Guadarrama, and Serguei Fomine*

Instituto de Investigaciones en Materiales, Universidad Nacional Autónoma deMéxico, Apartado Postal 70−360, CU, Coyoacán, Mexico DF 04510, México

Received: December 5, 2008; Revised Manuscript Received: January 16, 2009

The geometries of neutral, monooxidized, and monoreduced donor−acceptor tubular aggregates of cyclo[8]thiophene, cyclo[8](3,4-dicyanothiophene), and the corresponding donor−acceptor tubular nanoaggregates containing up to 4 repeating units were fully optimized at MPWB1K/3-21G* level of theory. The binding energies between macrocycles in neutral donor−acceptor tubular aggregates (77−84 kcal/mol) were found to be much higher compared to donor (43−45 kcal/mol) or acceptor (27−28 kcal/mol) aggregates. The oxidation or the reduction of the donor−acceptor tubular aggregates lead to a decrement in the binding energy. However, the reduction increases the binding in acceptor aggregates and decreases in donor ones, whereas the oxidation causes the opposite effect. In spite of a decrease in the binding energy in donor−acceptor aggregates in oxidized or reduced states, they remain the most thermodynamically stable formations. Donor−acceptor aggregates possess the lowest band gap among all studied systems (1.31 eV for the tetramer) and the photoexcitation of donor−acceptor aggregates results in almost complete electron transfer from donor to acceptor fragment, thus showing a very strong charge separation in the excited-state, which is highly desirable in materials with potential application in photovoltaic devices. Polaron cations are localized at donor fragments, whereas polaron anions are located at acceptor units.

Introduction

The current trend in research and development of novel materials to produce photovoltaic devices is aimed to find a convincing cost/efficiency compromise to make viable their use as power sources. The organic, polymer-based photovoltaic elements have introduced the potential of obtaining cheap and easy methods to produce energy from light.[1] Since 1986 when Tang[1b] accomplished a 1% power conversion efficiency with an organic photovoltaic cell based on low molecular weight organic thin-film photodetector, great advances have been made resulting in a variety of strategies for solar-cell improvements based on polymers.[2] Solar cells based on conjugated polymers alone have been promising candidates for use in low-cost electronics and photovoltaics;[3] however, with low quantum efficiency. Nevertheless, by mixing electron-donor-type polymers with suitable electron acceptors[4] highly efficient materials have been prepared. This is a very efficient way to break apart photoexcited excitons into free charge carriers. Another important strategy to increase the efficiency of solar cells is to decrease the band gap of organic semiconductors, allowing better overlap with the solar spectra.[5,6] The realization of these concepts are the mixtures of fullerenes (acceptor) with conjugated polymers (donor),[7,8] "double cable" polymers, where electron acceptor moieties are chemically attached to the donor polymer backbone to prevent the phase separation[9] or bulk heterojunction of two conjugated polymers[10] where one polymer bears the acceptor and the other donor functional groups. Polythiophenes are important materials for solar cells due to their excellent performance and power-conversion efficiencies.[11] It has been demonstrated that molecular architecture and increased dimensionality of polythiophene have important consequences on the electronic properties as it has been shown for 2D-macrocyclic,[12] disk- and starlike,[13] as well as for 3D-cruciform,[14] catenated,[15] and branched dendritic[16] oligothiophens. Theoretical calculations have also demonstrated that 2D-macrocyclic oligothiophens are able to form stable tubular aggregates due to $\pi-\pi$ stacking between macrocycles with the binding energy achieving 45 kcal/mol.[17] It was established that there exists a noticeable interaction between π-orbitals of individual macrocycles in tubular aggregates as follows from a decrease of the band gap with a number of repeating units in aggregates and the polaron delocalization toward tube axes in oxidized species. The aim of this study is to explore the stability and the electronic properties of tubular aggregates consisting of alternating donor and acceptor oligothiophene macrocycles using quantum chemistry tools. These aggregates could be potentially interesting as materials for solar cells due to such characteristics as: tunable band gap depending on the ionization potential (IP) of a donor and electron affinity (EA) of an acceptor, the absence of the phase separation due to possible thermodynamic stability of self-assembled aggregates, and efficient breaking apart photoexcited excitons into free charge carriers.

Computational Details. The modeling of complexes bonded by mostly dispersion interactions is a challenging task requiring methods taking into account dynamic correlation. It has been shown earlier[17] that MPWB1K functional performs very well for model oligothiophene dimers showing differences with MP2 optimized geometries of only 0.01−0.02 Å even for the most challenging interplane distances, whereas for the binding energies the difference was within a few tenths of a kcal/mol. It has also been shown that MPWB1K functional performed well for stacking interactions and H_2, Ne, and N_2 encapsulation into C60.[18] MPWB1K is based on the modified Perdew−Wang 1991 exchange functional[19] and Becke's 1995 meta correlation functional,[20] where meta means that it depends on kinetic energy density as well as the density and the gradient of density. MPWB1K incorporates 44% HF exchange. Therefore, all calculations were carried out using MPWB1K/3-21G* model with the *Gaussian 03* suit of programs.[21] MPWB1K functional is available in *Gaussian 03* through a combination of keywords;

10.1021/jp810722b CCC: $40.75
Published on Web 02/19/2009

TABLE 1: Calculated Interplane Distances in Tubular Aggregates (Å)

aggregate	1−2[a]	2−3[a]	3−4[a]
2CNC8	3.15−3.18		
2CNC8−C8	3.08−3.11		
4CNC8	3.21−3.25	3.21−3.27	3.21−3.25
4CNC8−C8	3.09−3.18	3.12−3.18	3.10−3.12
2CNC8$^+$	3.16−3.20		
2CNC8−C8$^+$	3.10−3.19		
4 CNC8$^+$	3.11−3.27	3.09−3.28	3.09−3.27
4CNC8−C8$^+$	3.09−3.19	3.13−3.16	3.13−3.18
2C8$^-$	3.12−3.13		
2CNC8$^-$	3.17−3.20		
2CNC8−C8$^-$	3.09−3.13		
4C8$^-$	3.10−3.12	3.11−3.12	3.04−3.13
4CNC8$^-$	3.20−3.27	3.21−3.29	3.20−3.28
4CNC8−C8$^-$	3.12−3.17	3.12−3.17	3.11−3.12

[a] The index numbers of macrocycles. In ***n*CNC8−C8** aggregates the first macrocycle is **CNC8**.

TABLE 2: Calculated Average Binding Energies between Macrocycles in Tubular Aggregates (kcal/mol)

aggregate	neutral	cation	anion
2C8	44.6[a]	50.1[a]	38.0
2CNC8	27.6	25.6	47.9
2CNC8−C8	83.7	59.6	69.7
4C8	42.9[a]	47.7[a]	40.0
4CNC8	26.9	25.6	40.1
4CNC8−C8	77.2	69.0	77.3

[a] Data used from ref 17.

mpwb95 and iop ($^3/_{76}$ = 0560004400). Restricted HF and unrestricted HF formalisms were used for closed- and opened-shell systems, respectively. Cyclo[8]thiophene, cyclo[8](3,4-dicyanothiophene), and their tubular aggregates containing up to 4 monomer units were fully optimized without any symmetry restrictions. Time-dependent (TD) DFT calculations were carried out using MPWB1K/3-21G* optimized geometry at B3LYP/6-31G* level to estimate the band gap of tubular aggregates. This level of theory reproduced very well experimental band gaps of linear oligothiophens.[17] Moreover, this model reproduces well the first excitation energy of donor−acceptor complex of aniline and *o*-chloranile (2.13 vs 2.04 eV[22]) that is of importance for correct description of the band gaps for tubular structures with alternated donor−acceptor units. Tubular aggregates of cyclo[8]thiophene, cyclo[8](3,4-dicyanothiophene) and their linear oligomers are denoted as ***n*C8**, ***n*CNC8**, and ***n*CNC8−C8**, where ***n*** is the number of cyclic fragments in the aggregate. Cation and anion radicals are referred to as + and − super indexes, respectively. The average binding energy (E_b) was calculated as $(E_t - E_c)/n - 1$, where E_c is the total electronic energy of a tubular aggregate, E_t is the sum of total electronic energies of monomer units, and n is the number of monomer units in the aggregate. The positive and negative charges were placed at a donor (**C8**) or acceptor (**CNC8**) unit respectively in case of charged aggregates.

Results and Discussion

Neutral Aggregates. Figure 1 and Table 1 show optimized geometries and interplane distances in oligocyclo[8]thiophene nanoaggregates. As seen from Table 1, the interplane distances increase in the order ***n*C8** (3.07 Å),[17] ***n*CNC8−C8**, and ***n*CNC8**, taking dimers as a reference. This effect is related with the difference in molecular volume between hydrogen atom and CN group. The difference in interplane distances between ***n*C8** and ***n*CNC8** is of 0.1−0.3 Å because of steric hindrances between CN groups of adjacent macrocycles. In the case of ***n*CNC8−C8** aggregates, the difference does not exceed 0.05 Å. Table 2 shows average binding energies in tubular aggregates. As seen there is a correlation between interplane distances and the binding energies for ***n*C8** and ***n*CNC8** aggregates. Thus, for ***n*CNC8** the binding energies (27−28 kcal/mol) are notoriously lower compared to ***n*C8** aggregates (39−45 kcal/mol)[17] reflecting larger interplane distances in ***n*CNC8** aggregates. The situation changes drastically for donor−acceptor aggregates ***n*CNC8−C8**. As seen from the Tables 1 and 2, in spite of the slightly larger interplane distances compared to ***n*C8**, the calculated binding energies in ***n*CNC8−C8** are much larger compared to ***n*C8** ranging from 83.7 kcal/mol for **2CNC8−C8** to 77.2 kcal/mol for **4CNC8−C8**. Because the interplane distances in ***n*CNC8-C8** and ***n*C8** aggregates are rather similar and the most of the binding energy in ***n*C8** aggregates should come from dispersion, one can approximately estimate the contribution from donor−acceptor interactions to ***n*CNC8−C8** binding energy as the difference between the binding energy in ***n*C8** and the corresponding ***n*CNC8−C8**. As seen in the case of ***n*CNC8−C8** aggregates, about half of the binding energy comes from donor−acceptor interactions. Therefore, alternating donor−acceptor aggregates are more stable thermodynamically than corresponding donor or acceptor counterparts. It has been shown earlier that in ***n*C8** aggregates there is a noticeable interactions between π-orbitals of macrocycles.[17] A similar trend holds for ***n*CNC8** and ***n*CNC8−C8** aggregates as well. As seen from Table 3, the band gap decreases with the number of repeating units, resembling that observed for conjugated polymers. When comparing the band gap of tubular aggregates with the same number of repeating units, it is seen that donor−acceptor aggregates show the smallest band gap (1.31 eV for **4CNC8−C8**), whereas the largest band gaps are for ***n*C8** aggregates. The larger conjugated system in ***n*CNC8** aggregates results in lower excitation energies for all ***n*CNC8** systems compared to ***n*C8** ones. Moreover, the larger conjugated system in the **CNC8** monomer is responsible for the faster decrease of the band gap for ***n*CNC8** compared to ***n*C8** (Table 3). Thus, for ***n*C8** the band gap drops from 2.60 eV for **C8** to 2.52 eV for **4C8**,[17] whereas for ***n*CNC8** from 2.56 to 1.71 eV, respectively. However, the most notorious is a decrease of the band gap observed for donor−acceptor aggregates. According to TD-DFT calculations, in all cases the most important contribution to the excitation energy comes from HOMO−LUMO transition. Figure 2 shows HOMO and LUMO of ***n*CNC8−C8** tubular aggregates. As seen from the Figure 2, the HOMO of aggregates is located at **C8** units, whereas the LUMO is at the **CNC8** one. Thus, the electron is transferred from donor to acceptor unit, stabilizing the excited-state and contributing to a decrease of excitation energy. According to calculations, the excitation in ***n*CNC8−C8** aggregates leads to almost complete electron transfer from donor to acceptor fragment. Figure 3 shows the charge distribution in S0 and S1 states of ***n*CNC8−C8** tubular aggregates. Thus, the Mulliken charges of the donor unit in the ground and excited states of **2CNC8−C8** were found to be of +0.21 and +1.03 respectively, reflecting an increase of the dipole moment from 5.46 D for the ground state to 18.6 D for the excited state. In **4CNC8−C8** aggregate there are two nonequivalent **C8** and **CNC8** units. The Mulliken charges of outer and inner **C8** fragments in S0 state were found to be of +0.23 and +0.16 respectively, whereas for **CNC8**, −0.11 and −0.28, respectively. In the S1 state, the electron transfer occurs from the outer **C8** to the outer **CNC8** fragment, changing the

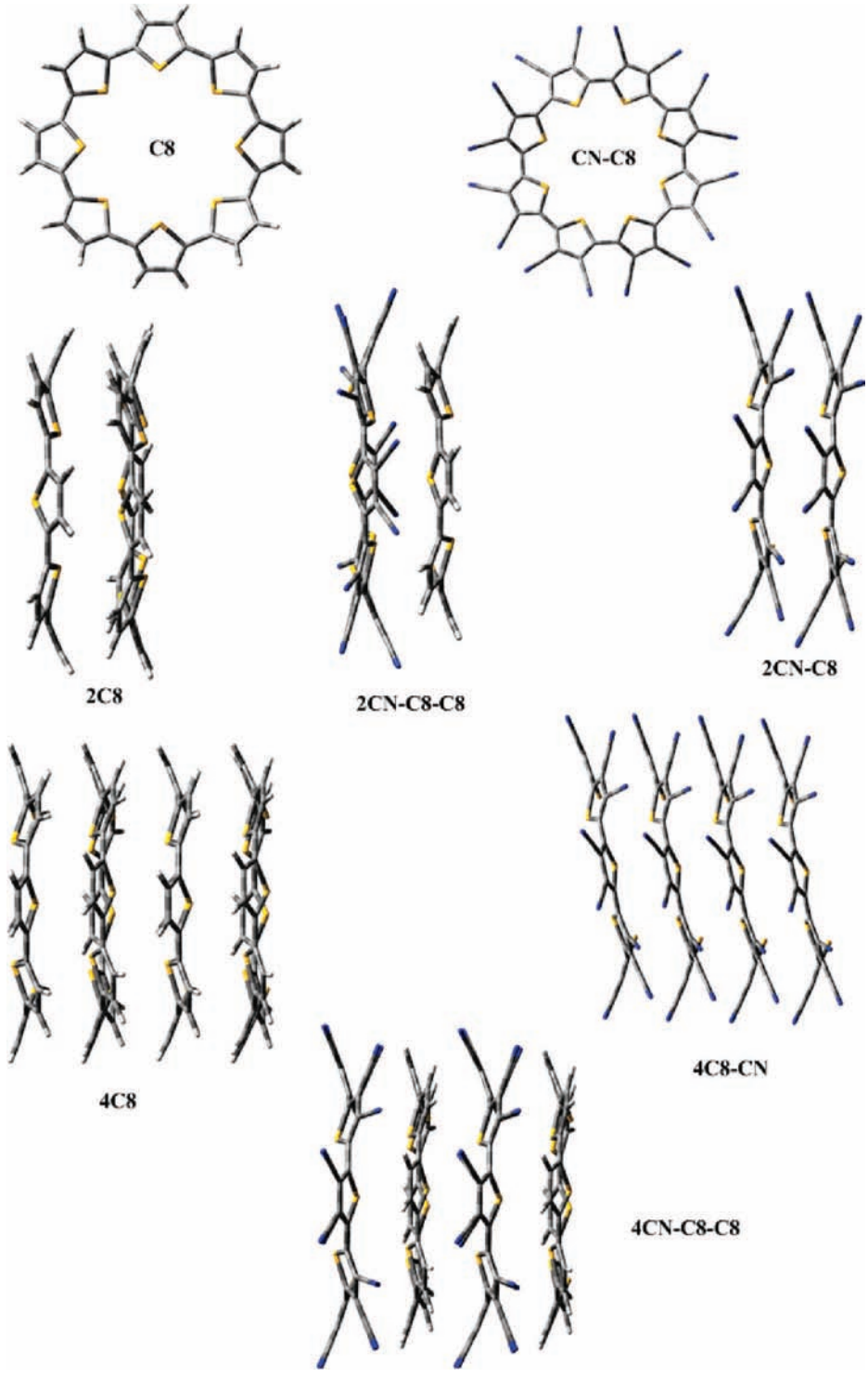

Figure 1. MPWB1K/3-21G* optimized geometries of neutral tubular aggregates.

Mulliken charges of the corresponding macrocycles to +1.14, +0.14, −0.30, and −0.98, respectively (Figure 3). This charge transfer leads to an increase of dipole moment from 6.8 D in the ground to 50.0 D in the excited state, corresponding to almost complete electron transfer. The photoelectron transfer from the outer donor to the outer acceptor unit reflects the maximum stabilization of the formed exciton because the outer donor and acceptor groups should have the lowest **IP** and the highest **EA**, respectively (Table 3). Therefore, in the case of larger ***n*CNC8−C8** aggregates the photoelectron transfer should occur from the outer donor to the outer acceptor unit, thus favoring the charge separation. The photoexcitation of acceptor tubular aggregates ***n*CNC8** does not result in significant charge separation. Similar situation is observed for the donor ***n*C8** aggregates.[17] It is interesting to compare the calculated interplane distances in donor acceptor tubular aggregates, and these are found for linear oligothiophens as the polythiophene model. Thus, the shortest C−C distance found between nearest molecules in adjacent layers of hexathiophene crystal[23] is of 3.82 Å, which is more than 0.5 Å large compared to these found for studied tubular aggregates (Table 1). The denser packing of thiophene units in tubular aggregates compared to linear oligothiophenes implies better charge mobility in these systems.

TABLE 3: Vertical (IP_v, EA_v) and Adiabatic (IP_a, EA_a) Ionization Potentials and Electron Affinity, respectively. Relaxation Energies (λ_+, λ_-), and the Band Gaps (E_g) of Tubular Aggregates (eV)

aggregate	IP_a	IP_v	EA_a	EA_v	E_g	λ_+[a]	λ_-[b]
C8	6.33[c]	6.58[c)]	0.94	0.61	2.60	0.25	0.33
CNC8	9.18	9.31	3.81	3.69	2.56	0.13	0.12
2C8	6.06[c)]	6.21[c)]	0.65	0.52	2.53	0.15	0.13
2CNC8	9.27	9.34	4.69	4.60	2.00	0.07	0.09
2CNC8−C8	7.38	7.53	3.20	3.12	1.39	0.15	0.08
4C8	5.68[c]	5.82[c)]	0.56	0.46	2.52	0.14	0.10
4CNC8	9.36	9.58	5.52	5.00	1.71	0.22	0.52
4CNC8−C8	7.39	7.52	3.83	3.80	1.31	0.13	0.03

[a] The energy difference between the vertical and adiabatic ionization potentials. [b] The energy difference between the adiabatic and vertical electron affinity. [c] Data taken from ref 17.

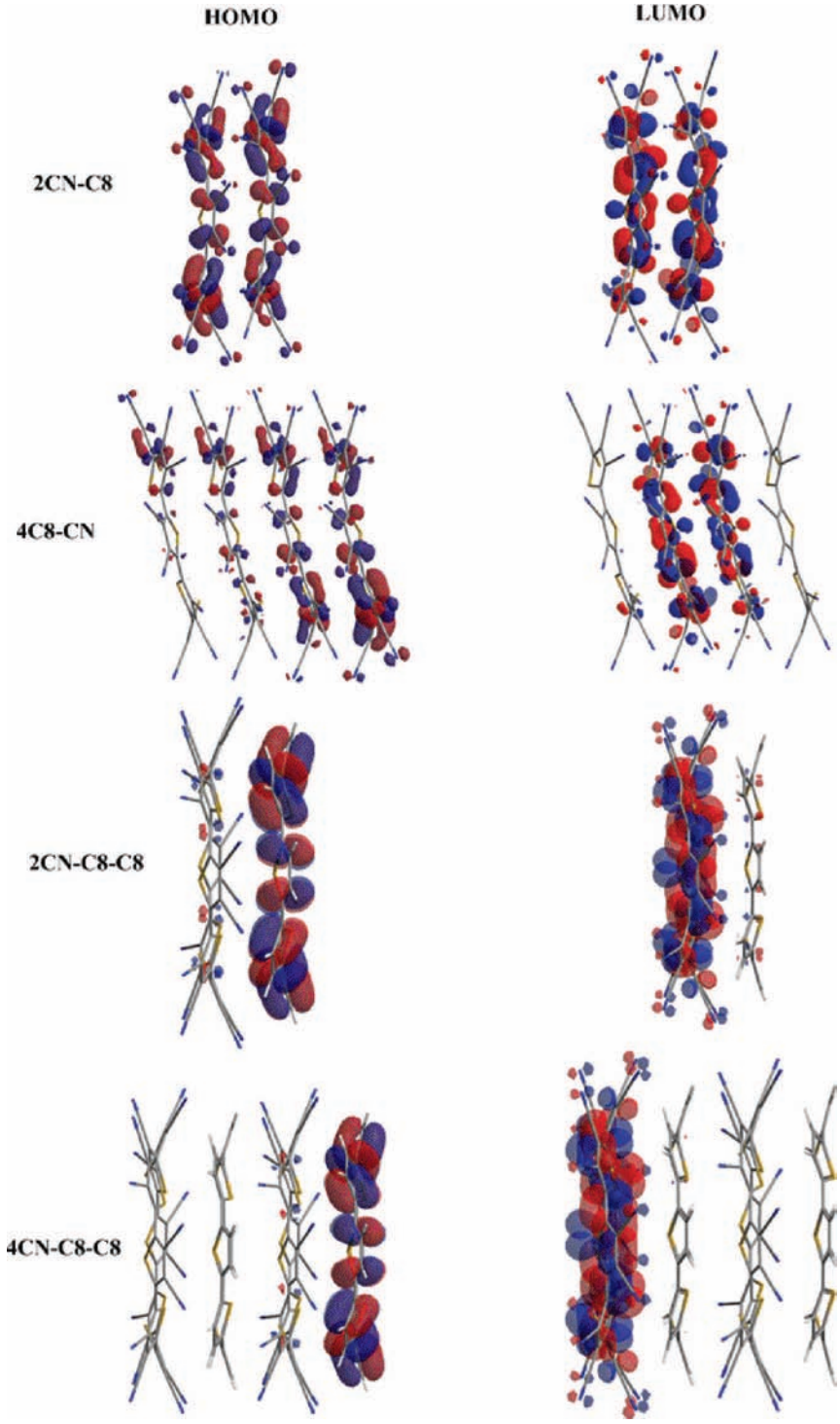

Figure 2. HOMO and LUMO of tubular ***n*CNC8−C8** aggregates calculated at B3LYP/6-31G*// MPWB1K/3-21G* level.

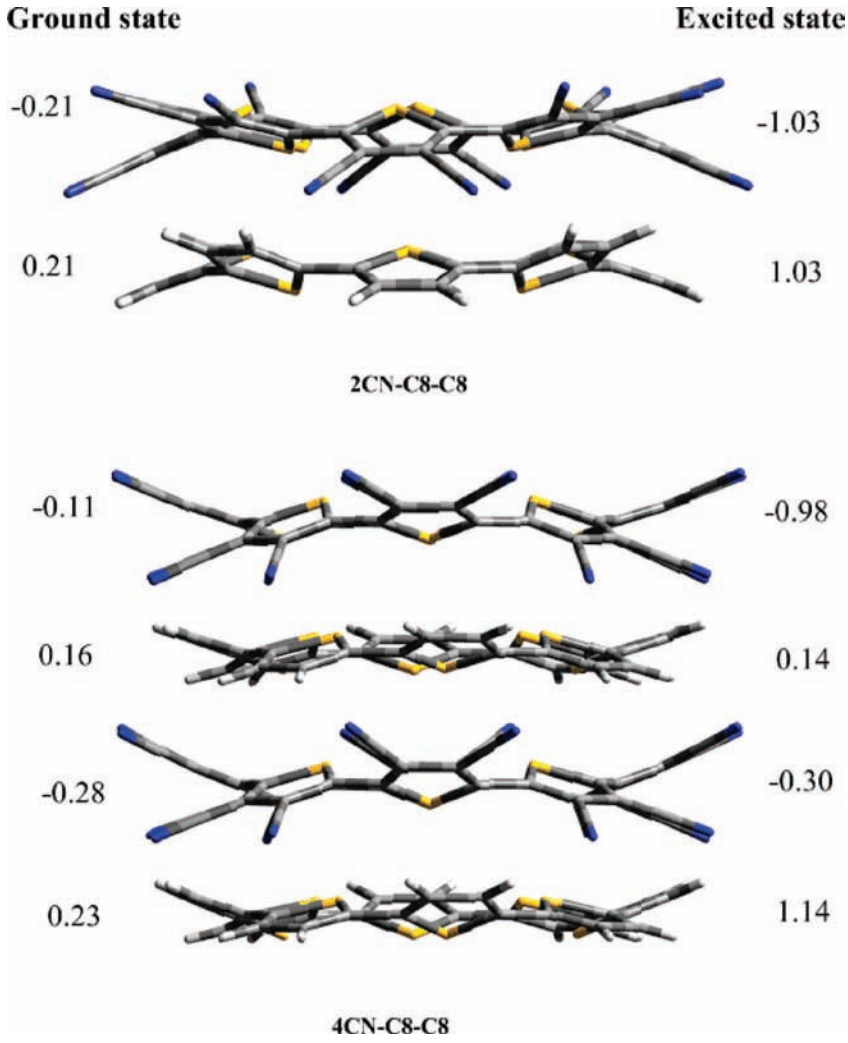

Figure 3. Mulliken charges at monomers of **2CNC8−C8** and **4CNC8−C8** tubular aggregates in S0 and S1 states respectively, calculated at TD-B3LYP/6-31G*// MPWB1K/3-21G* level.

Cations. The first step in doping of a conjugated polymer is the formation of a cation or anion radical (polaron). These species are responsible for the charge transport phenomenon by a hopping-type mechanism between adjacent molecules or chains accompanied by geometric relaxation.[24]

Table 3 shows vertical ($\mathbf{IP_v}$) and adiabatic ($\mathbf{IP_a}$) ionization potentials for studied aggregates. The difference between vertical and adiabatic **IP** or between adiabatic and vertical electron affinity (**EA**) represents the relaxation energy (λ_+ and λ_-, respectively) that is a measure of mobility of polaron in conjugated system.

Generally, the relaxation energies decrease with oligomer chain length as a result of greater charge delocalization in a longer oligomer.[25] $\mathbf{IP_v}$ reflects the conjugation in a neutral molecule and the ability of the electronic system to stabilize positive charge. As seen from Table 3, the **IP**s both vertical and adiabatic decrease in the order ***n*CNC8**, ***n*CNC8−C8**, ***n*C8** as it could be expected from the chemical structure of the aggregates, from the acceptor ***n*CNC8** to the donor ***n*C8**. Unlike ***n*C8** where **IP**s drop with the number of repeating units,[17] they do not depend on the aggregate size for ***n*CNC8−C8** and slightly increase for ***n*CNC8**. This unusual behavior could be a result of cation polarons localization at only one macrocycle in ***n*CNC8−C8** and ***n*CNC8**, as follows from Figure 4, compared to ***n*C8**.[17] As it has been shown earlier[17] in the case of ***n*C8** aggregates, the relaxation energy (λ_+) passes through a minimum with the number of the repeating units due to the interplay between polaron delocalization and the deformability of the aggregate. Similar trends were observed for ***n*CNC8** aggregates (Table 3). As seen, the smallest λ_+ is observed for **2CNC8**. However, λ_+ for **4CNC8** is higher compared to donor−acceptor **4CNC8−C8**. This fact is easily understood if comparing the binding energies in the corresponding aggregates. As seen from Table 2, the binding energy in **4CNC8−C8** is significantly higher compared to **4CNC8** ones, thus decreasing the deformability of the donor−acceptor tubular aggregates.

The ionization leads to a noticeable change in the binging energies of the aggregates. It has been shown earlier[17] that monoionization increases the binding energies in ***n*C8**. The situation, however, is completely different for ***n*CNC8−C8** and ***n*CNC8** aggregates where ionization decreases the binding energies (Table 2). This effect is very strong for **2CNC8−C8** where the binding energy decreases by 24.1 kcal/mol. The reason can be understood inspecting the polaron cation distributions (Figure 4). As seen in ***n*CNC8−C8$^+$**, the polaron is located almost completely at donor **C8** unit, thus decreasing donor properties of **C8** fragment. However, for ***n*CNC8$^+$** aggregates the decrease of binding energy on ionization is almost imperceptible being of 1−2 kcal/mol. It is noteworthy that, even though the binding energy of ***n*CNC8−C8$^+$** drops drastically for cation radicals, it is still higher than the binding energies of the corresponding cationic homoaggregates ***n*C8$^+$** and ***n*CNC8$^+$**,

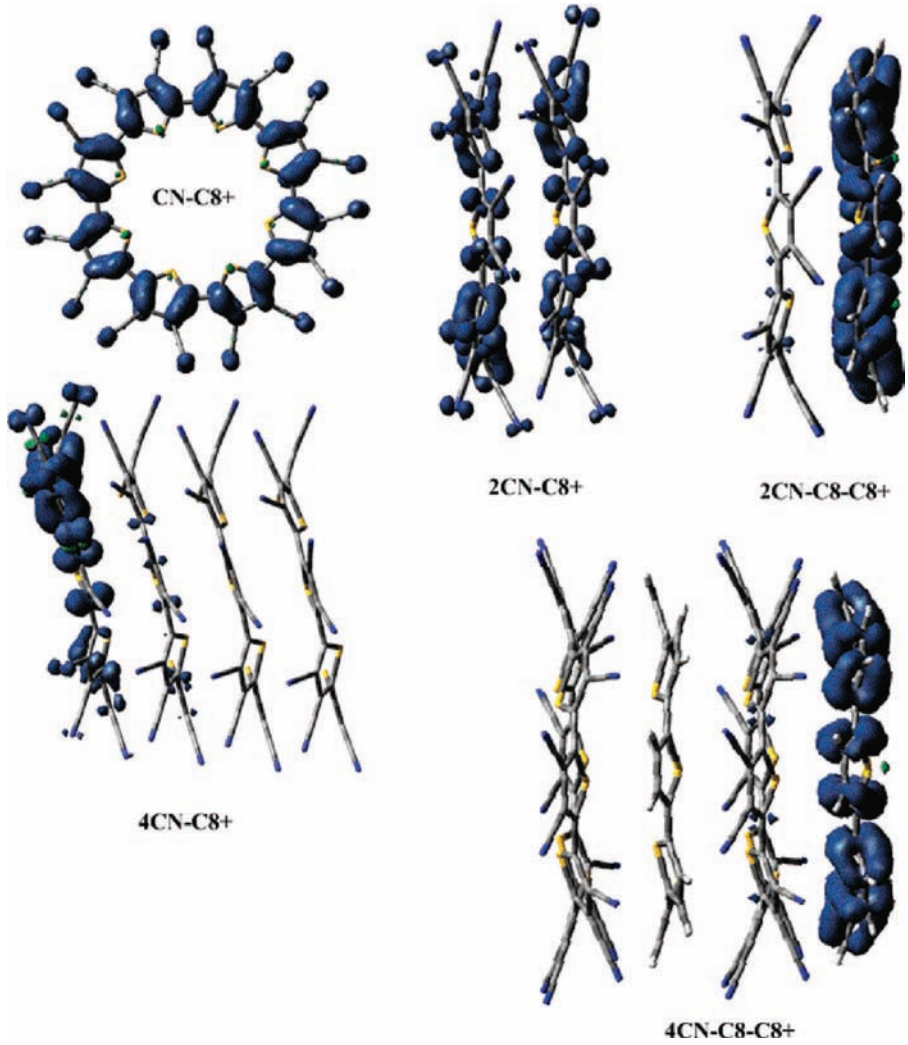

Figure 4. MPWB1K/3-21G* optimized geometries and unpaired spin density distribution in cation radicals of tubular aggregates.

thus avoiding the dissociation of ***n*CNC8−C8**$^+$ into a mixture of ***n*C8**$^+$ and ***n*CNC8**$^+$ aggregates. Unlike ***n*C8**$^+$ where polarons were delocalized essentially over entire tubular structure with a maximum at the central macrocycles[17] the polaron cations are much more localized in ***n*CNC8−C8**$^+$ and ***n*CNC8**$^+$ aggregates. In ***n*CNC8−C8**$^+$, the polaron cation is always localized at outer donor **C8** unit. In the case of the **2CNC8** aggregate, the polaron cation is delocalized over two units, whereas for **4CNC8** the cation−radical is localized mostly at the outer **CNC8** macrocycle. For tetramers, the lowest λ_+ is calculated for donor−acceptor **4CNC8−C8**, implying best mobility of polaron cations in this system. This can be attributed to the strongest binding in these aggregates and, therefore, more rigid structure. As seen from the Tables 1 and 2, a drop of the binding energies in cations is accompanied by a slight increase of the interplane distances in **2CNC8**$^+$ and **2CNC8−C8**$^+$, whereas for the tetramers there is observed no clear correlation of interplane distances and binding energies.

Anions. The doping of a conjugated systems by electron-donors to produce polaron anions is determined by their **EA**s. Table 3 shows vertical and adiabatic **EA**s of the corresponding tubular aggregates. **EA**s increase with the number of repeating units for ***n*CNC8−C8** and ***n*CNC8** aggregates but drop for ***n*C8**. ***n*CNC8** aggregates were found to be very good electron acceptor with adiabatic electron affinities reaching 5.52 eV for **4CNC8** (Table 3). The binding energies calculated for reduced species (anion radicals) differ from these of neutral and cation radicals (Table 2). As seen, the reduction of the neutral aggregates decreases the binding energy for ***n*C8**$^-$ and increases for ***n*CNC8**$^-$. As it could be expected, the difference is higher for dimers and lower for tetramers. In the case of donor−acceptor aggregates, the reduction leads to a moderate decreases of the binding energies for **2CNC8−C8**$^-$, whereas for **4CNC8−C8**$^-$ the binding energy is almost not affected by the reduction. As seen from the Table 2, the weakest binding between macrocycles for anions is observed for ***n*C8**$^-$, whereas the strongest for ***n*CNC8−C8**$^-$. According to calculations, the reduction of neutral donor−acceptor aggregates will not lead to their dissociation to give donor and acceptor aggregates because donor−acceptor aggregates maintain the strongest binding energy among all studied complexes. Figure 5 shows the distribution of polaron anions in tubular aggregates. As seen in the case of ***n*CNC8−C8**$^-$ aggregates, the polaron anion is localized mostly at the acceptor **CNC8** fragment. This decreases the acceptor properties of **CNC8** unit and, therefore, reduces the binding energy in anion−radical. It is noteworthy that the distribution of polaron anions in acceptor ***n*CNC8**$^-$ is very similar to the distribution of polaron cations in donor ***n*C8**[17] and conversely. This fact can be explained by the following effect. Thus, in donor aggregates the terminal macrocycle should have highest **EA**, whereas in acceptor aggregates the terminal macrocycle has the lowest **IP** due to the influence of the neighboring macrocycle. Therefore, the cation polaron and the

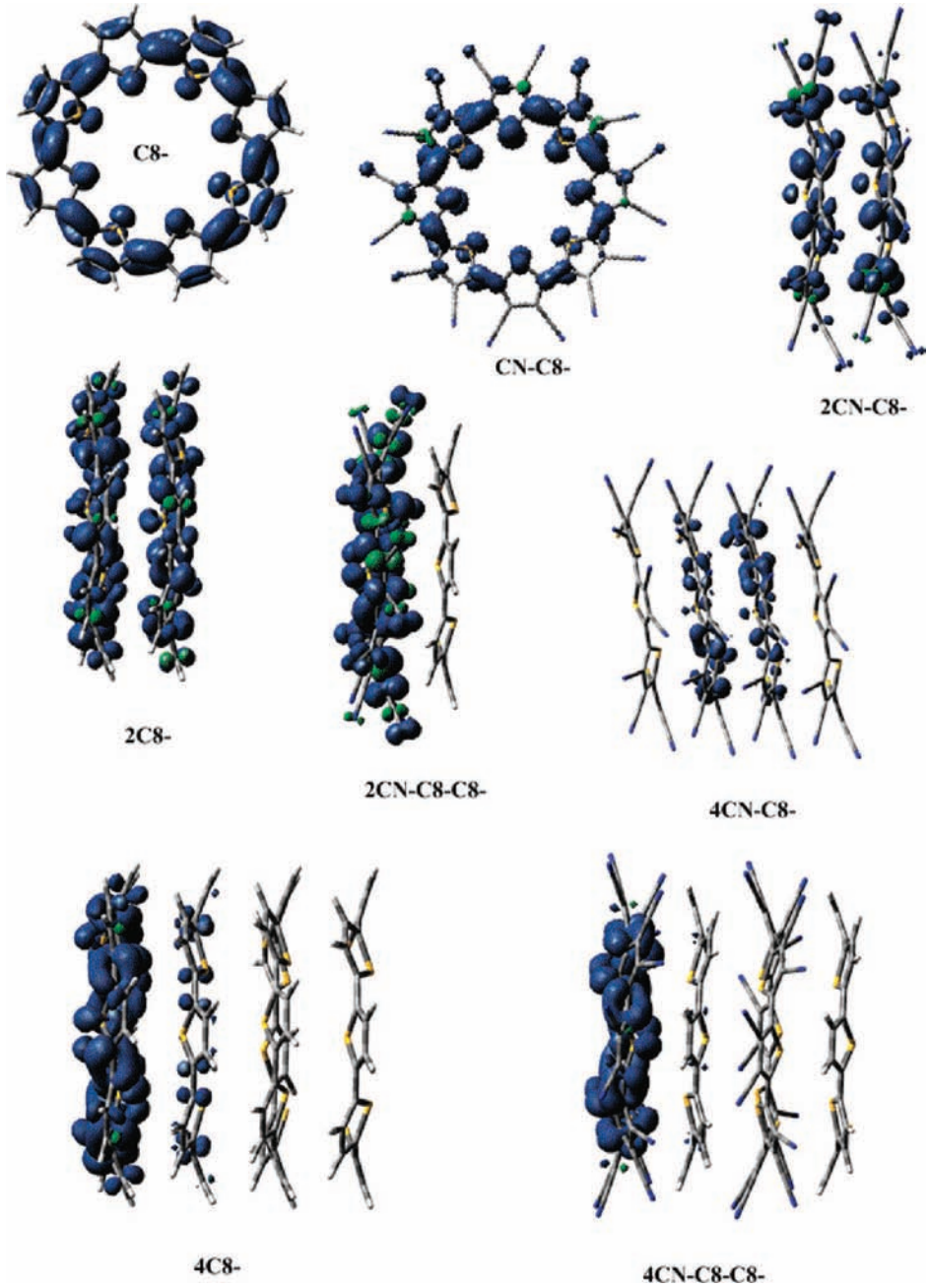

Figure 5. MPWB1K/3-21G* optimized geometries and unpaired spin density distribution in anion radicals of tubular aggregates.

anion polaron are mostly localized at terminal macrocycles in acceptor and donor aggregates, respectively.

In the case of dimers **2C8**$^-$ and **2CNC8**$^-$, polaron anions are delocalized over two fragments (Figure 5); however, whereas for tetramer **4CNC8**$^-$ the polaron anion is delocalized symmetrically over two central fragments in the case of **4C8**$^-$, the polaron anion is localized predominantly at the outer **C8** macrocycle. When inspecting the relaxation energies (λ_-) for anion−radicals one can see that unlike λ_+, for all tubular aggregates λ_- decrease with the number of repeating units, except for **4CNC8**$^-$. As seen, ***n*CNC8−C8** aggregates show the lowest λ_- out of all studied tubular aggregates that could be related to the high binding energy in these complexes and, therefore, low deformability of these systems. **4CNC8**$^-$ shows unusually high λ_-. It seems that the difference in delocalization patterns of polaron anions compared to other anions is responsible for this. Unlike **4CNC8−C8**$^-$ and **4C8**$^-$ where polarons are mostly localized at only one terminal macrocycle, in **4CNC8**$^-$ the delocalization pattern of polaron anion involves all central parts of the tubular aggregate. Therefore, the deformation caused by polaron anion in **4CNC8**$^-$ must be notoriously higher compared to **4CNC8−C8**$^-$ and **4C8**$^-$ because in **4CNC8−C8**$^-$ the polaron is delocalized over several macrocycles binded by relatively weak intermolecular forces, whereas in the case of **4CNC8−C8**$^-$ and **4C8**$^-$ the polaron is located over rigid macrocycles with low deformability. As a consequence, λ_- is higher in **4CNC8−C8**$^-$ compared to **4CNC8−C8**$^-$and **4C8**$^-$. This hypothesis is also confirmed by the fact that **4CNC8−C8**$^+$ showing that the polaron delocalization pattern similar to **4CNC8−C8**$^-$ has higher relaxation energy compared to **4C8**$^-$.[17]

Concluding Remarks. The calculation demonstrated that donor−acceptor ***n*CNC8−C8** aggregates are thermodynamically more stable than the corresponding donor ***n*C8** and acceptor ***n*CNC8** aggregates and, therefore, could be a target for self-assembling. According to calculations, the additional stability

of ***n*CNC8−C8** aggregates comes from donor−acceptor interactions representing about half of the total binding energy. The formation of donor−acceptor aggregates reduces greatly (by about 1 eV) the band gap of the conjugated system compared to donor or acceptor aggregates. The photoexcitation of donor−acceptor aggregates leads to the electron transfer from the outer donor to the outer acceptor, leading to the formation of an excited-state with very strong charge separation. The delocalization patterns of polaron cations and polaron anions depend on the type of tubular aggregates. Thus, polaron anions are much better delocalized in acceptor aggregates, whereas polaron cations are in the donor ones. In case of donor−acceptor aggregates, polaron cationes are localized at the donor fragments, whereas polaron anions are localized at the acceptor ones, thus favoring the charge separation for photogenerated charge carriers. When inspecting the relaxation energies (λ_- and λ_+) for tetramers, one can see that they are lowest for donor−acceptor ***n*CNC8−C8** aggregates, implying higher charge mobility compared to other studied types of tubular aggregates. In conclusion, donor−acceptor tubular aggregates could be a promising new class of photovoltaic materials due to a small and adjustable band gap, strong charge separation in the excited state, and high possible mobility of the charge carriers as follows from their low relaxation energies.

Acknowledgment. This research was carried out with the support of Grant 49290 from CONACyT. We acknowledge the support of DGSCA, UNAM, for using supercomputer Kan-Balam. We thank an anonymous reviewer whose review greatly helped to improve the manuscript.

Supporting Information Available: Optimized cartesian coordinates. This material is available free of charge via the Internet at http://pubs.acs.org.

References and Notes

(1) (a) Sariciftci, N. S.; Smilowitz, L.; Heeger, A. J.; Wudl, F. *Science* **1992**, *258*, 1474. (b) Tang, C. W. *Appl. Phys. Lett.* **1986**, *48*, 183.

(2) Bundgaard, E.; Krebs, F. C. *Sol. Energy Mater. Sol. Cells* **2007**, *91*, 954.

(3) Gunes, S.; Neugebauer, H.; Sariciftci, N. S. *Chem. Rev.* **2007**, *107*, 1324.

(4) (a) Koster, L. J. A.; Mihailetchi, V. D.; Bloom, P. W. *Appl. Phys. Lett.* **2006**, *88*, 93511. (b) Scharber, M. C.; Mühlbacher, D.; Koppe, M.; Denk, P.; Waldauf, C.; Heeger, A. J.; Brabec, C. J. *Adv. Mater.* **2006**, *18*, 789.

(5) (a) Dhanabalan, A.; van Duren, J. K. J.; van Hal, P. A.; van Dongen, J. L. J.; Janssen, R. A. J. *Adv. Funct. Mater.* **2001**, *11*, 255. (b) Meng, H.; Cheng, Y.; Wudl, F. *Macromolecules* **2001**, *34*, 1810. (c) Meng, H.; Tucker, D.; Chaffins, S; Chen, Y. S.; Helgeson, R.; Dunn, B.; Wudl, F. *Adv. Mater.* **2003**, *15*, 146.

(6) (a) van Duren, J. K. J.; Dhanabalan, A.; van Hal, P. A.; Janssen, R. A. J. *Synth. Met.* **2001**, *121*, 1587. (b) Campos, L. M.; Tontcheva, A.; Gunes, S.; Sonmez, G.; Neugebauer, H.; Sariciftci, N. S.; Wudl, F. *Chem. Mater.* **2005**, *17*, 4031. (c) Sonmez, G.; Shen, C. K. F.; Rubin, Y.; Wudl, F. *Adv. Mater.* **2005**, *17*, 897.

(7) Yu, G.; Heeger, A. J. *J. Appl. Phys.* **1995**, *78*, 4510.

(8) Halls, J. J. M.; Walsh, C. A.; Greenham, N. C.; Marseglia, E. A.; Friend, R. H.; Moratti, S. C.; Holmes, A. B. *Nature* **1995**, *376*, 498.

(9) Cravino, A.; Sariciftci, N. S. *J. Mater. Chem.* **2002**, *12*, 1931.

(10) Yu, G.; Heeger, A. J. *J. Appl. Phys.* **1998**, *78*, 4510.

(11) Ma, W.; Yang, C.; Gong, X.; Lee, K.; Heeger, A. J. *Adv. Funct. Mater.* **2005**, *15*, 1617.

(12) (a) Krömer, J.; Rios-Carreras, I.; Fuhrmann, G.; Musch, C.; Wunderlin, M.; Debaerdemaeker, T.; Mena-Osteritz, E.; Bäuerle, P. *Angew. Chem.* **2000**, *112*, 3623. (b) Krömer, J.; Rios-Carreras, I.; Fuhrmann, G.; Musch, C.; Wunderlin, M.; Debaerdemaeker, T.; Mena-Osteritz, E.; Bäuerle, P. *Angew. Chem., Int. Ed.* **2000**, *39*, 3481. (c) Mena-Osteritz, E.; Bäuerle, P. *Adv. Mater.* **2001**, *13*, 243. (d) Fuhrmann, G.; Bäuerle, P. *Chem. Commun.* **2003**, 926. (e) Bäuerle, P.; Fischer, T.; Bidlingmeier, B.; Rabe, J. P.; Stabel, A. *Angew. Chem., Int. Ed.* **1995**, *34*, 303–307.

(13) (a) Nicolas, Y.; Blanchard, P.; Levillain, E; Allain, M; Mercier, N.; Roncali, J. *Org. Lett.* **2004**, *6* (2), 273. (b) Sun, X.; Liu, Y.; Chen, S.; Qiu, W.; Yu, G.; Ma, Y.; Qi, T.; Zhang, H.; Xu, X.; Zhu, D. *Adv. Funct. Mater.* **2006**, *16*, 917. (c) Kopidakis, N.; Mitchell, W. J.; van de Lagemaat, J.; Ginley, D. S.; Rumbles, G.; Shaheen, S. E.; Rance, W. L. *Appl. Phys. Lett.* **2006**, *89*, 103524.

(14) Bilge, A.; Zen, A.; Forster, M.; Li, H.; Galbrecht, F.; Nehls, B. S.; Farrell, T.; Neher, D.; Scherf, U. *J. Mater. Chem.* **2006**, *16*, 3177.

(15) (a) Ammann, M.; Rang, A.; Schalley, C. A.; Bäuerle, P. *Eur. J. Org. Chem.* **2006**, 1940. (b) Bäuerle, P.; Ammann, M.; Wilde, M.; Götz, G.; Mena-Osteritz, E.; Rang, A.; Schalley, C. A. *Angew. Chem., Int. Ed* **2007**, *46*, 363.

(16) Jennings, W. B.; Farrell, B. M.; Malone, J. F. *Acc. Chem. Res.* **2001**, *34*, 885.

(17) Flores, P.; Guadarrama, P.; Ramos, E.; Fomine, S. *J. Phys. Chem. A* **2008**, *112*, 3996.

(18) Slanina, Z.; Pulay, P.; Nagase, S. *J. Chem. Theory Comput.* **2006**, *2*, 782.

(19) Perdew, J. P.; Wang, Y. *Phys. Rev. B* **1992**, *45*, 13244.

(20) Becke, A. D. *J. Chem. Phys.* **1996**, *104*, 1040.

(21) Frisch, M. J.; Trucks, G. W.; Schlegel, H. B.; Scuseria, G. E.; Robb, M. A.; Cheeseman, J. R.; Zakrzewski, V. G. J. ; Montgomery, A.; Stratmann, R. E., Jr.; Burant, J. C.; Dapprich, S.; Millam, J. M.; Daniels, A. D.; Kudin, K. N.; Strain, M. C.; Farkas, O.; Tomasi, J.; Barone, V.; Cossi, M.; Cammi, R.; Mennucci, B.; Pomelli, C.; Adamo, C.; Clifford, S.; Ochterski, J.; Petersson, G. A.; Ayala, P. Y.; Cui, Q.; Morokuma, K.; Malick, D. K.; Rabuck, A. D.; Raghavachari, K.; Foresman, J. B.; Cioslowski, J.; Ortiz, J. V.; Baboul, A. G.; Stefanov, B. B.; Liu, G.; Liashenko, A.; Piskorz, P.; Komaromi, I.; Gomperts, R.; Martin, R. L.; Fox, D. J.; Keith, T. Al-Laham, M. A.; Peng, C. Y.; Nanayakkara, A.; Challacombe, M.; Gill, P. M. W.; Johnson, B.; Chen, W.; Wong, M. W.; Andres, J. L.; Gonzalez, C.; Head-Gordon, M.; Replogle, E. S.; Pople, J. A. *Gaussian 03*, Rev. E.01; Gaussian, Inc.: Wallingford, CT, 2004.

(22) Bhattacharya, S. *Chem. Phys. Lett.* **2007**, *446*, 199.

(23) Horowitz, G.; Bachet, B.; Yassar, A.; Lang, P.; Demanze, F.; Fave, J.-L.; Garnier, F. *Chem. Mater.* **1996**, *7*, 1337.

(24) (a) Brédas, J. L.; Calbert, J. P.; da Silva Filho, D. A.; Cornil, J. *Proc. Natl. Acad. Sci. U.S.A.* **2002**, *99*, 5804. (b) Cornil, J.; Beljonne, D.; Calbert, J. P.; Brédas, J. L. *Adv. Mater.* **2001**, *13*, 1053.

(25) Hutchison, G. R.; Ratner, M. A.; Marks, T. J. *J. Am. Chem. Soc.* **2005**, *127*, 2339.

JP810722B